Separation Science and Technology
Publication details, including instructions for authors and subscription information:
http://www.informaworld.com/smpp/title~content=t713708471

Chiral Separation of R,S-α-Tetralol by Simulated Moving Bed

Michal Zabka[a]; Mirjana Minceva[a]; Pedro Sá Gomes[a]; Alírio E. Rodrigues[a]
[a] Faculty of Engineering, Department of Chemical Engineering, Laboratory of Separation and Reaction Engineering (LSRE), University of Porto, Porto, Portugal

To cite this Article Zabka, Michal , Minceva, Mirjana , Gomes, Pedro Sá and Rodrigues, Alírio E.(2008) 'Chiral Separation of R,S-α-Tetralol by Simulated Moving Bed', Separation Science and Technology, 43: 4, 727 — 765
To link to this Article: DOI: 10.1080/01496390701870689
URL: http://dx.doi.org/10.1080/01496390701870689

Separation Science and Technology, 43: 727–765, 2008

ISSN 0149-6395 print/1520-5754 online
DOI: 10.1080/01496390701870689

Chiral Separation of R,S-α-Tetralol by Simulated Moving Bed

Michal Zabka, Mirjana Minceva, Pedro Sá Gomes, and Alírio E. Rodrigues

Faculty of Engineering, Department of Chemical Engineering, Laboratory of Separation and Reaction Engineering (LSRE), University of Porto, Porto, Portugal

Abstract: This work deals with chiral separation by Simulated Moving Bed (SMB) chromatography. A simulation package is used to predict the effect of the operating variables on the process performance. The "separation volume" methodology is used to study effect of the presence of mass transfer resistances presented by different particle sizes on operating conditions of the SMB unit with emphasis to the net flow in zone I and IV in terms of interstitial velocity ratio (γ_1 and γ_4). The experimental operation of the a pilot plant SMB unit LICOSEP 12–26 (Novasep, France) is carried out for the separation of enantiomers of R,S-α-Tetralol using the chiral adsorbent CHIRALPAK AD with particle size 20 μm. To obtain real insight to operation of the SB unit Licosep 12–26 the mathematical model accounts for all dead volumes inside of the SMB unit and time delay in shifting of injection and withdrawal points. Experimental and theoretical results based on the SMB model are compared in terms of process performance parameters and internal concentration profiles.

Keywords: Simulated moving bed, CHIRALPAK AD, liquid chromatography, mathematical modeling, chiral alcohol

Received 28 June 2007, Accepted 4 November 2007

Address correspondence to Alírio E. Rodrigues, Faculty of Engineering, Department of Chemical Engineering, Laboratory of Separation and Reaction Engineering (LSRE), University of Porto, Rua Dr. Roberto Frias s/n, Porto 4200-465, Portugal. Tel.: 351 225081671; Fax: 351 22 5081674; E-mail: arodrig@fe.up.pt

INTRODUCTION

A long time ago, chromatography was limited only to special applications and considered as a very expensive tool in the production of fine chemicals. The Simulated Moving Bed technology (SMB) was developed and patented in the 1960's by UOP (1, 2) and has been widely used at very large scale in the petrochemical and sugar industry. Nowadays, many chiral stationary phases are available for analytical purposes but only a few materials are widely used for preparative enantioseparation. By far alkyl-phenylcarbamate derivatives of cellulose and amylose are the most used chiral stationary phases on the preparative scale (3, 4) mainly due to a wide range of resolved racemates with various functional groups. These chiral phases were invented by Okamoto (5, 6) and commercialized by Daicel Chemical Industries Ltd (7, 8).

In the early 1990's when the scaling down of a simulated moving bed unit was introduced by Separex, SMB chromatography with a combination of chiral stationary phases became a key technology for the isolation and purification of chiral drugs and natural products on a large scale (9–17).

Batch chromatography was widely used in the separation of fine chemicals as a highly selective technique. However, it is well known that batch chromatography disadvantages are high product dilution, high eluent consumption, and non-effective utilization of adsorbent. SMB chromatography is a multi-column continuous chromatographic binary separation technique involving a simulated counter-current movement of the adsorbent and liquid (1, 12). Therefore, higher throughput, purity and yield relative to the batch chromatography are achieved. There are already several publications that show better performance of the SMB in comparison with other available large-scale separation processes (18–24).

The adsorbent is one of the most important parts of the SMB system, as it is related to the productivity and the economic feasibility of the whole process. There are numerous different chiral stationary phases available in the market and used mainly for analytical separation; however, only a few stationary phases have been utilized in preparative chromatography, a consequence of the requirements for chemical and mechanical stability and the stationary phase lifetime. Great versatility in enantioseparation has been shown for derivatized cellulose and amylose stationary phases (3).

The effect of the particle size on the separation performance of a simulated moving bed was studied from various points of view (25–28). In this study the effect of the particle size on the performance of the SMB unit was undertaken using a separation volume concept. The enantioseparation of the secondary alcohol R,S-α-Tetralol on chiral adsorbent CHIRALPAK AD was used. It is worth pointing out that we kept constant and equal column lengths inside the system, constant adsorption equilibrium parameters for each particle size involved, and target purity value of 99%. Separation of α-Tetralol on chiral adsorbent CHIRALPAK AD was experimentally validated in the Licosep SMB pilot plant 12–26.

Principle of Simulated Moving Bed

The SMB operation is usually described based on the equivalent True Moving Bed (TMB) unit. The TMB unit (Fig. 1a) is typically a system where the solid and the fluid phase are flowing in opposite directions. Along the column are situated two inlet (feed and eluent) and two outlet (extract and raffinate) streams, which are splitting the unit into four sections and hence allowing the separation of both the species. The solid flow rate is constant along the TMB unit while the liquid flow rate is different in each section as a result of different flow rates of each inlet and outlet stream, which have to be adequately chosen. Each section plays a different role in the entire separation process of a binary feed mixture:

- In section 1, between the eluent port and the extract port, the more retained species (A) must be desorbed from the adsorbent and therefore moved upwards to the extract port, so the adsorbent can be clean when entering section 4.
- In section 2, between the extract and feed ports, the less retained species (B) must move upwards to avoid contamination of the extract stream. In this section B is desorbed from the adsorbent and displaced by the more retained species (A), which will move downwards to the extract port together with the solid phase.
- In section 3, between the feed and raffinate ports, the more retained species (A) must be adsorbed and moved downwards with solid phase; consequently it does not reach the raffinate outlet, whereas the less retained species (B) is moved upwards with the liquid to the raffinate outlet.

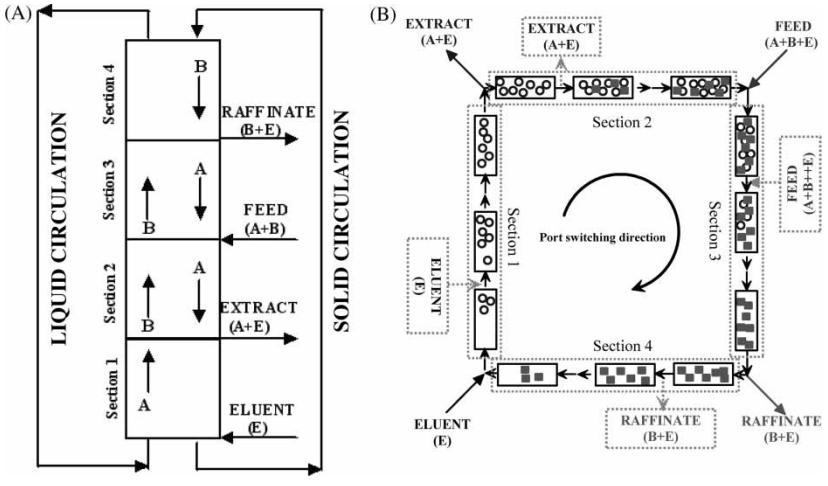

Figure 1. (a) Schematic diagram of the TMB and (b) schematic diagram of the SMB.

- In section 4, between the raffinate and eluent ports, the less retained species (B) must be adsorbed onto the solid phase, ensuring that the eluent leaving section 4 is clean and can be recycled to section 1.

The TMB technology approach is not technically feasible due to the problems connected with transport of the solid phase through the system (1). These issues have been overcome by discretization of the single TMB column into fixed bed columns with identical length, the counter current movement of the solid and the liquid phase is simulated by shifting of the of inlet and outlet ports at discrete time intervals in the direction of the fluid flow, which is the basis of the SMB technology (Fig. 1b)

MATHEMATICAL MODELING OF SIMULATED MOVING BED

The SMB can be modeled using two modelling approaches: the equivalent TMB and the real SMB approach (29). The difference between both approaches is in the stationary regime. In the TMB the steady state is reached whereas in the SMB it is a cyclic steady state; thus in each section there is an identical transient during each switching period. The cyclic steady state (CSS) is reached after a certain number of cycles, but the system state is still varying over the time because of the periodic movement of the inlet and outlet ports along the columns.

The mathematical models of the equivalent TMB system and the real SMB system is summarized in Table 1. Both models consider axial dispersion flow for the liquid phase, linear driving force (LDF) for the intraparticle mass transfer rate, and multicomponent adsorption equilibrium described by the non-stoichiometric linear + Langmuir isotherm. Moreover, the mathematical model of the equivalent TMB system considers plug flow for the solid phase.

The overall mass transfer coefficient of component i in j section of TMB is given by

$$k_{ovij} = \frac{1}{1/k_{ext_{ij}} + 1/k_{int_i}} \tag{19}$$

where the $k_{ext_{ij}}$ (cm/s) and k_{int_i} (cm/s) are the external (film) and internal mass transfer coefficient of component i in j section of TMB. The internal mass transfer coefficient was calculated by the expression suggested by Glueckauf (30) was used and is given by $k_{int_i} = 5D_{p_i}/R_p$ where $D_{p_i} = \varepsilon_p D_{m_i}/\tau$ where R_p (cm) is the particle radius, ε_p is the particle porosity (see Table 2), D_{m_i} (cm^2/s) molecular diffusivity, and τ is the tortuosity factor.

The external (film) mass transfer coefficient, k_{extij} was calculated from: $Sh_{ij} = k_{extij} d_p/D_{m_i} = 1.09/\varepsilon\ (Sc_i\ \mathrm{Re}_j)^{1/3}$, where Sc and Re were calculated by $Sc_i = \eta/\rho D_{m_i}$; $\mathrm{Re}_j = \rho v_j\, \varepsilon d_p/\eta$, where ρ (g/cm^3) is the mobile phase

Table 1. Model equations for the transie TMB model and SMB model

TMB model equations	SMB model equations
Mass balance in a volume element of the section j	Mass balance in a volume element of the column k
$\varepsilon \frac{\partial C_{ij}}{\partial t} = \varepsilon D_{L_j} \frac{\partial^2 C_{ij}}{\partial z^2} - \varepsilon v_j \frac{\partial C_{ij}}{\partial z} - (1-\varepsilon)\frac{3}{R_p} k_{ovij}(C_{ij} - \bar{C}_{p_{ij}})$ (1)	$\varepsilon \frac{\partial C_{ik}}{\partial t} = \varepsilon D_{Lk} \frac{\partial^2 C_{ik}}{\partial z^2} - \varepsilon v_k^* \frac{\partial C_{ik}}{\partial z} - (1-\varepsilon)\frac{3}{R_p} k_{ovik}(C_{ik} - C_{p_{ik}})$ (10)
Particle mass balance	Particle mass balance
$\varepsilon_p \frac{\partial \bar{C}_{p_{ij}}}{\partial t} + \frac{\partial \bar{q}_{ij}}{\partial t} = u_s \left[\varepsilon_p \frac{\partial \bar{C}_{p_{ij}}}{\partial z} + \frac{\partial \bar{q}_{ij}}{\partial z} \right] + \frac{3}{R_p} k_{ov_{ij}}(C_{ij} - \bar{C}_{p_{ij}})$ (2)	$\varepsilon_p \frac{\partial C_{p_{ik}}}{\partial t} + \frac{\partial q_{ik}}{\partial t} = \frac{3}{R_p} k_{ovik}(C_{ik} - C_{p_{ik}})$ (11)
Initial conditions	Initial conditions
$t = 0;\ C_{ij} = \bar{C}_{p,ij} = 0;\ \bar{q}_{ij} = 0$ (3)	$t = 0;\ C_{ik} = \bar{C}_{p,ik} = 0;\ q_{ik} = 0$ (12)
Boundary conditions	Boundary conditions
$z = 0;\ v_j C_{ij} - D_{ax,j} \left.\frac{\partial C_{ij}}{\partial z}\right\|_{z=0} = v_j C_{ij}^{in}$ (4a)	$z = 0;\ v_k^* C_{ik} - \varepsilon D_{ax,k} \left.\frac{\partial C_{ik}}{\partial z}\right\|_{z=0} = v_k^* C_{ik,F}$ (13a)
$z = L_j; \left.\frac{\partial C_{ij}}{\partial z}\right\|_{z=L_j} = 0;\ \bar{C}_{p_{ij,L_j}} = \bar{C}_{p_{ij+1,0}};\ j = 1:3;\ \bar{q}_{ij,L_j} = \bar{q}_{ij+1,0};$	$z = L_j; \left.\frac{\partial C_{ik}}{\partial z}\right\|_{z=L_k} = 0$ (13b)
$j = 1{:}3\ \bar{C}_{p_{i4,L_j}} = \bar{C}_{p_{i1}};\quad \bar{q}_{i4,L_j} = \bar{q}_{i1}$ (4b)	
Multicomponent adsorption equilibrium isotherm	Multicomponent adsorption equilibrium isotherm
$q_{ij}^* = H_i C_{p_{ij}} + \frac{q_m b_i C_{p_{ij}}}{1 + \sum_{i=1}^{n} b_i C_{p_{ij}}}$ (5)	$q_{ik}^* = H_i C_{p_{ik}} + \frac{q_m b_i C_{p_{ik}}}{1 + \sum_{i=1}^{n} b_i C_{p_{ik}}}$ (14)

(*continued*)

Table 1. Continued

TMB model equations		SMB model equations	
Global mass balances in sections			
Eluent node:		Eluent node:	
$\nu_4 + \nu_E = \nu_1$	(6a)	$\nu_4^* + \nu_E = \nu_1^*$	(15a)
$c_{i,4}^{out}\nu_4 = c_{i,1}^{in}\nu_1$	(6b)	$c_{i,4}^{out}\nu_4^* = c_{i,1}^{in}\nu_1^*$	(15b)
Feed node:		Feed node:	
$\nu_2 + \nu_F = \nu_3$	(7a)	$\nu_2^* + \nu_F = \nu_3^*$	(16a)
$c_{i,2}^{out}\nu_2 + c_{i,F}\nu_F = c_{i,3}^{in}\nu_3$	(7b)	$c_{i,2}^{out}\nu_2^* + c_{i,F}\nu_F = c_{i,3}^{in}\nu_3^*$	(16b)
Extract node:		Extract node:	
$\nu_1 - \nu_X = \nu_2$	(8a)	$\nu_1^* - \nu_X = \nu_2^*$	(17a)
$c_{i,1}^{out} = c_{i,2}^{in} = c_{i,X}$	(8b)	$c_{i,1}^{out} = c_{i,2}^{in} = c_{i,X}$	(17b)
Raffinate node:		Raffinate node:	
$\nu_3 - \nu_R = \nu_4$	(9a)	$\nu_3^* - \nu_R = \nu_4^*$	(18a)
$c_{i,3}^{out} = c_{i,4}^{in} = c_{i,R}$	(9b)	$c_{i,3}^{out} = c_{i,4}^{in} = c_{i,R}$	(18b)

[a]In above equation i relates to the component in the mixture (i = S-α-Tetralol and R-α-Tetralol); j relates to the TMB section number ($j = 1, 2, 3, 4$) and k relates to the SMB number of columns ($k = 1, 2, \ldots$).

Table 2. Operating conditions and model parameters for SMB and equivalent TMB

	Sections				
	I	II	III	IV	dp μm
SMB					
Liquid flow rates, Q_j^* (cm^3/min)	41.00	35.35	38.85	33.98	
Switching time t^* (min)			3.50		
TMB					
Liquid flow rates Q_j, (cm^3/min)	34.93	29.28	32.78	27.91	
Solid flow rate Q_S (cm^3/min)			9.10		
Ratio fluid and solid interstitial velocities in TMB, γ_j	5.757	4.826	5.403	4.600	
External flow rates					
Eluent = 7.02 (cm^3/min)					
Extract = 5.65 (cm^3/min)					
Feed = 3.50 (cm^3/min)					
Raffinate = 4.87 (cm^3/min)					
$D_m = 2.8 \times 10^{-5}$ (cm^2/s)					
K_{ov} (cm/s)					
0.0061					20
0.0031					40
0.0020					60

Column: Diameter = 2.6 cm, Length of column: 10 cm. Configuration of columns: 1:2:2:1; Particle size: 20 μm, 40 μm, 60 μm; External porosity: $\varepsilon = 0.4$; Total porosity: $\varepsilon_T = 0.61$; Particle porosity, $\varepsilon_p = 0.35$; Total feed concentration:4 g/dm^3.

density, η (Pa · s) is the viscosity, v_j (m/s) is the interstitial velocity in section, j, and ε is the bed porosity.

The molecular diffusivities of the adsorbate R,S-(±)-α-Tetralol were approximated by the Wilke-Chang equation (31) and extended to mixed solvents by Perkins and Geankoplis (32) D_{m_i} (cm^2/s) $= 7.4 \times 10^{-8}$ $T\sqrt{\phi M}/\eta\ V_{m_i}{}^{0.6}$, where T (K) is the absolute temperature, η its viscosity (cP), which was calculated according to the Teja and Rice method (33) for liquid mixture. The molar volume of the adsorbate at its normal boiling temperature V_{m_i} (cm^3/mol) was estimated by the Le Bas method (34). The molecular diffusivity of each enantiomer is identical and therefore the internal mass transfer coefficient k_{int_i} is identical for both enantiomers.

The fluid velocities and inlet concentrations in each section were calculated from the inlet and outlet nodes balances given in Table 1.

The equivalence between the TMB and the SMB approach is obtained by keeping constant the liquid interstitial velocity relative to the solid interstitial velocity. The equivalence expressed in terms of interstitial velocities is $v_j = v_j^* - u_s$, where $u_s = L_c/t^*$, and $v_j = Q_j/\varepsilon\ A$ and v_j^* is the interstitial liquid velocity in the TMB and SMB, respectively, A is the cross section

area of the bed, and Q_j is the TMB liquid flow rate. The solid velocity in TMB u_s is related to the switching time period of the SMB model t^*.

This equivalence expressed in terms of SMB and TMB flow rates is given by: $Q_j^* = Q_j + \varepsilon/(1-\varepsilon)Q_s$ with $Q_s = (1-\varepsilon)V/t^*$, where Q_j^* is liquid flow rate in section j of the SMB, Q_s is the TMB solid flow rate V is the volume of one SMB column.

Extra-Column Dead Volume

Extra-column dead volume increases the residence time in the SMB unit made of the dead volume and the chromatographic column compared to the retention time in a chromatographic column alone. In addition, the concentration profiles in the SMB unit are more dispersive due to back mixing in the dead volume itself. Hence, the SMB mathematical model was extended to account for the extra-column dead volume (see Fig. 2) so called Licosep model. The flow in the connection tubes was modelled by an axial dispersion flow according to the following equation (35, 36)

$$\frac{\partial C_i}{\partial t} = -\frac{Q_{pc_j}}{A_{pc}}\frac{\partial C_i}{\partial z} + D_{Lpc}\frac{\partial^2 C_i}{\partial z^2} \tag{20}$$

Initial conditions:

$$t = 0 \quad C_i = 0 \tag{21}$$

Boundary conditions

$$z = 0 \quad \nu_{pc} C_i - D_{Lpc}\left.\frac{\partial C_i}{\partial z}\right|_{z=0} = \nu_{pc} C_{i,F} \tag{22a}$$

$$z = L_{pc_j}\left.\frac{\partial C_i}{\partial z}\right|_{z=L_{pc}} = 0 \tag{22b}$$

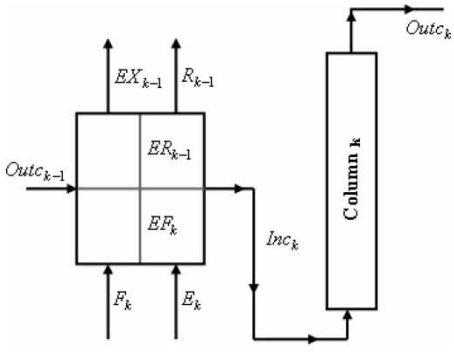

Figure 2. Detail view to the connection of columns in the SMB unit Licosep 12-26.

where Q_{pc_j} is the liquid flow rate in the pipe, A_{pc} is the cross-section area of the pipe, C_i is the species concentration, D_{Lpc} is the axial dispersion, and L_{pc} is the length of the pipe.

The axial dispersion in pipes was approximated by the following correlation for laminar flow [37]: $D_{Lpc} = Q_{pc}^2 d_{pc}^2 / 192\, A_{pc}^2 D_m$, where d_{pc} is the diameter of pipes and D_m is the molecular diffusivity of α-Tetralol in mobile phase heptane/2-propanol (95/5).

Performance Parameters

The performance of the SMB unit for the separation of the binary mixture (racemic mixture) is usually characterized by the following parameters: purity, recovery, solvent consumption, and productivity per unit of the adsorbent volume. The definitions of all performance parameters are given by:

Purity (%) of R-Tetralol in extract and S-Tetralol in raffinate stream:

$$PU_X = 100 C_X^R / (C_X^R + C_X^S) \tag{23a}$$

$$PU_R = 100 C_R^S / (C_R^R + C_R^S) \tag{23b}$$

Recovery (%) of R-Tetralol in extract and S-Tetralol in raffinate stream:

$$RE_X = 100 Q_X C_X^R / Q_F C_F^R \tag{24a}$$

$$RE_R = 100 Q_R C_R^S / Q_F C_F^S \tag{24b}$$

Eluent consumption (dm^3/g):

$$SC = (Q_E + Q_F)/Q_F (C_F^S + C_F^R) \tag{25}$$

Productivity ($g/h\ dm^3$):

$$PR_X = Q_X C_X^R / V_{ads} \tag{26a}$$

$$PR_R = Q_R C_R^S / V_{ads} \tag{26b}$$

It must be pointed out that C_X^R, C_R^S in the SMB unit are average concentrations over one complete cycle.

Numerical Solution of Model Equations

TMB and SMB model equations (Eqs. 1–18; Eqs. 20–22) were solved using the gPROMS software package (38). The mathematical models involve a system of partial differential and algebraic equations. The axial domain was discretized by a third order orthogonal collocation method in finite elements (OCFEM) comprising two interior collocation points and 40 elements per

column and 5 elements per pipe. An absolute and relative tolerance of 10^{-5} was used. CSS in Licosep unit was considered when the global error (16, 39) (the sum of the relative errors between the average concentration of each component in the extract and raffinate streams for the two consecutive interactions) was lower than 1%.

SIMULATION RESULTS

Influence of Operating Conditions (Switching Time and Particle Size)

The effect of the switch time period (t^*) on the SMB performance is studied for three different sizes of the adsorbent particles, leading to different internal mass transfer rate. For this purpose, the equivalent TMB steady state model was used.

The adsorption equilibrium isotherm for the enantiomers of R,S-α-Tetralol on the chiral adsorbent CHIRALPAK AD is given by (40, 41):

$$q_S^* = 1.14\, C_S + \frac{23.6 \times 0.077\, C_s}{1 + 0.077\, C_S + 0.042\, C_R} \tag{27a}$$

$$q_R^* = 2.47\, C_R + \frac{23.6 \times 0.042\, C_R}{1 + 0.077\, C_S + 0.042\, C_R} \tag{27b}$$

with q_i^* in g/dm^3 of adsorbent and C_i in g/dm^3.

The operating conditions and model parameters for TMB and SMB models are summarized in Table 2. The system contains six columns with configuration of columns per section 1:2:2:1. The particle sizes of the adsorbent were 20 μm, 40 μm and 60 μm. Performance parameters have been calculated according to Eqs. 23–24. Molecular diffusivity, D_m of R,S-α-Tetralol and overall mass transfer coefficients, k_{ov} for each particle size (averaged over all section) are reported in Table 2. The influence of the switch time period on the system performance (purity and recovery) packed with particle sizes 20 μm, 40 μm and 60 μm is reported in Figs. 3, 4, and 5, respectively.

Decreasing the switch time period in the SMB system in relation to the reference case (Table 2) leads to increase of the solid flow rate and decrease of the internal liquid flow rates in equivalent TMB; and as a result, the less retained component (S-α-Tetralol) is moving downwards and pollutes the extract stream, the more retained species (R-α-Tetralol) is also moving downwards and is recycled together with the solid phase to section 4 and pollutes the raffinate stream. In the opposite case when the switching time in the SMB system is increased in relation to the reference case (Table 2) the solid flow rate is decreasing and the internal liquid flow rates are increasing. In this case, the less retained species is recycled with the liquid phase to the section 1 polluting the extract stream and the more retained species is moving upwards with the liquid phase and pollutes the raffinate stream.

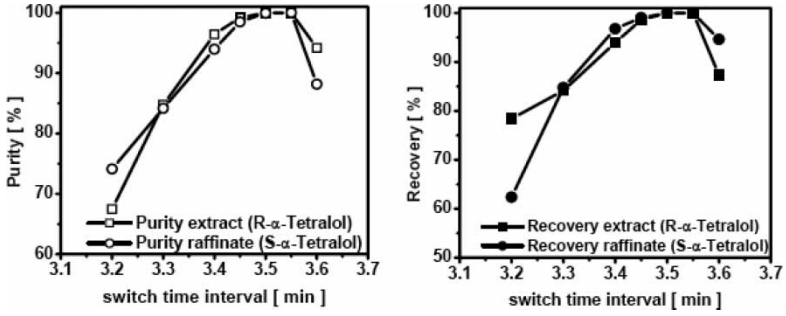

Figure 3. Effect of switching time interval on the purity and recovery on the particle size 20 μm.

It can be also observed that for switching time between 3.45 and 3.55 min the purity and recovery for both product streams are above 99% when using particle size 20 μm and 40 μm. However, in the same range of switching time and using particle size 60 μm the purity and recovery of the products are above 97%.

The internal concentration profiles for the particle sizes 20 μm, 40 μm and 60 μm with the switching time, $t^* = 3.5$ min are shown in Fig. 6 a,b,c, respectively. Bigger particle size leads to higher mass transfer resistance and more dispersed internal concentration profiles, which has an influence on the SMB performance parameters.

Prediction of Separation Volume and Influence of Particle Size

The equilibrium theory and the steady-state model of TMB has been one of the most common strategy applied to obtain the separation region in nonlinear

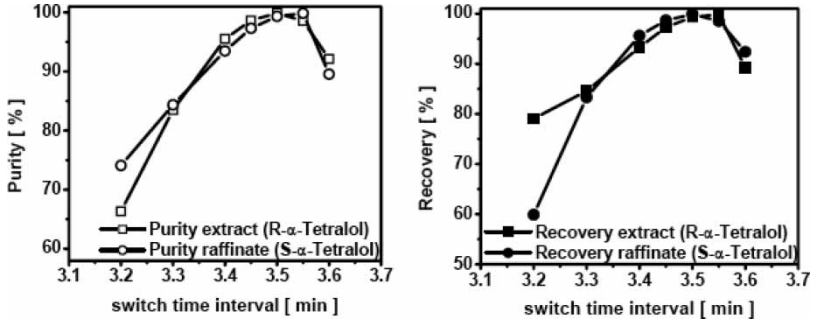

Figure 4. Effect of switching time interval on the purity and recovery on the particle size 40 μm.

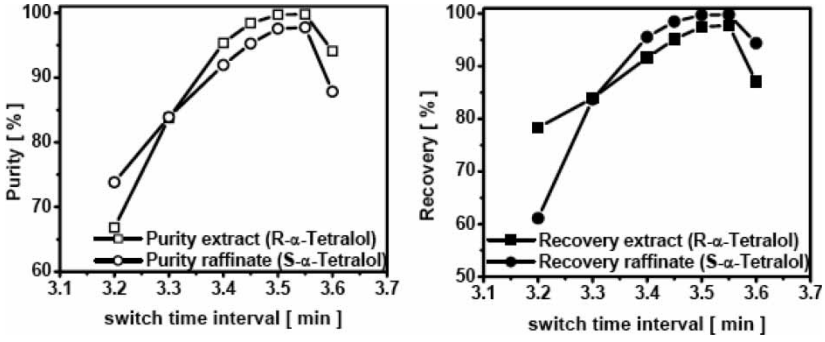

Figure 5. Effect of switching time interval on the purity and recovery on the particle size 60 μm.

systems (42–49). On the other hand such separation regions do not show the influence of the mass transfer resistance caused by particle size used (50, 51). Nevertheless, the equilibrium theory can be still used for preliminary estimations of SMB operating conditions (52).

The intraparticle mass transfer and its effect on SMB performance for linear system was introduced by Rodrigues et al. (53). The separation

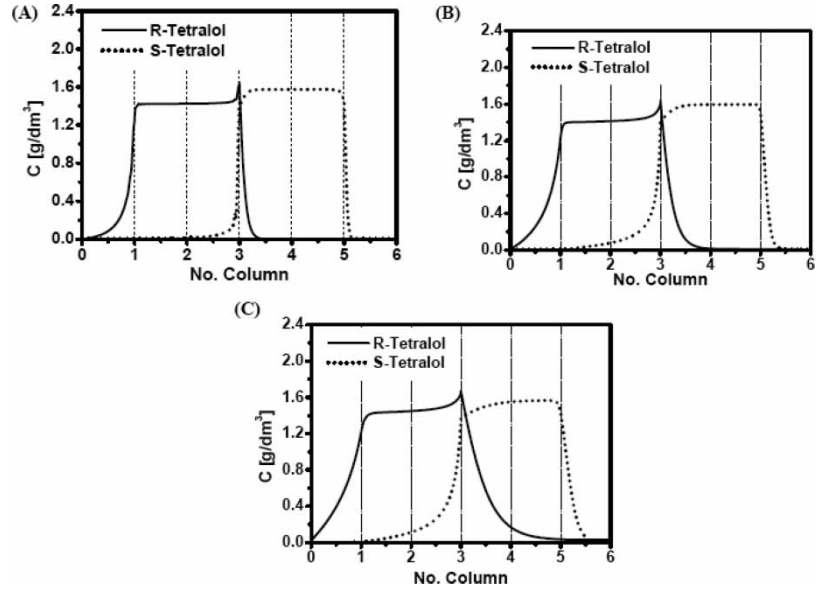

Figure 6. Effect of the particle size on the TMB concentration profile: (A) $d_p = 20$ μm, (B) $d_p = 40$ μm; (C) $d_p = 60$; operating conditions and model parameters in Table 2.

region size in the presence of the mass transfer limitations is reduced in comparison to that obtained by the equilibrium model, therefore new limiting liquid flow rates should be established. Therefore the methodology of "separation volumes" (51) was established, in order to better determine and optimize the operating conditions of the SMB system.

To withdraw the less adsorbed compound S-α-Tetralol (S) in the raffinate stream it must move upwards in section 1, 2, and 3 and move downwards in section 4. The more retained compounds R-α-Tetralol (R) is withdrawn in extract stream, it must move in section 1 upwards and in section 2, 3, and 4 downwards. Therefore, the following constraints expressed in terms of the net fluxes must be fulfilled:

$$\frac{Q_1 c_{R1}}{Q_s q_{R1}} > 1 \tag{28}$$

$$\frac{Q_2 c_{R2}}{Q_s q_{R2}} < 1; \frac{Q_2 c_{S2}}{Q_s q_{S2}} > 1 \tag{29}$$

$$\frac{Q_3 c_{R3}}{Q_s q_{R3}} < 1; \frac{Q_2 c_{S3}}{Q_s q_{S3}} > 1 \tag{30}$$

$$\frac{Q_4 c_{S4}}{Q_s q_{S4}} < 1 \tag{31}$$

For SMB process under nonlinear conditions (isotherm), the determination of flow rates in order to obtain the separation region is not straightforward in contrast with linear isotherm. This is mainly due to fact that ratio C_j/q_j in net fluxes given by (Eqs. 28–31) are concentration dependent since the adsorbed concentration of one species is depending on the concentration of both species occurring in the fluid phase.

The separation volumes for separation of α-tetralols by chiral adsorbent with different particle sizes have been determined numerically using steady state TMB model.

Construction of Separation Region

The separation of racemic mixture of R,S-α-Tetralol using the chiral adsorbent CHIRALPAK AD with particle size 20 μm 40 μm and 60 μm was considered. The adsorption isotherm is given by Eqs. (27 a, b).

The operating conditions will be expressed in terms of γ_j values given for each section j in system: $\gamma_j = \nu_j/u_s$ representing the ratio between the interstitial liquid velocity and solid phase velocity. The γ_j values are directly related to the SMB operating conditions given by $u_s = L_c/t^*$ and $\nu_j = \nu_j^* - u_s$, where ν_j^* the SMB interstitial liquid velocity.

Complete desorption of the more retained species and clean adsorbent must be obtained at the entrance of section 1. Therefore, the low liquid

concentrations of both species are expected in section 1; both species will be in linear range of the isotherm. On the other hand, the lower concentration is leading to longer retention times and hence the switching time must be selected in such a way that it will be greater than the retention time of the more retained compound at the maximum flow rate in this section. As pointed out above the optimal switch time period is 3.5 min.

The retention time of the more retained component can be calculated by

$$t_{RI} = \frac{\varepsilon V}{Q_I^*}\left(1 + \frac{1-\varepsilon}{\varepsilon}\varepsilon_p + \frac{1-\varepsilon}{\varepsilon}K_R\right) \tag{32}$$

where K_R is the initial slope of the isotherm for the more retained compound, $K_R = 3.46$; V is the volume of the column in the SMB system ($V = 53.09\ \mathrm{cm}^3$); for particle porosity see Table 2. To guarantee the condition stated by equilibrium theory (54) the following criterion must be full filled: $\gamma_1 > \gamma_{1,\min} = 1 - \varepsilon/\varepsilon\,(K_R + \varepsilon_p) = 5.715$, which corresponds to a minimal SMB flow rate in section 1 equal to 40.741 $\mathrm{cm}^3/\mathrm{min}$.

The function of section 4 is to regenerate the liquid phase so the less retained compounds must move downwards to be recovered in the raffinate node. The flow rate in the section four can be approximated as

$$Q_4^* = \frac{\varepsilon V}{t^*}\left(1 + \frac{1-\varepsilon}{\varepsilon}\varepsilon_p + \frac{1-\varepsilon}{\varepsilon}\frac{\Delta q_S^{*F}}{\Delta C_S^F}\right) \tag{33}$$

where $\Delta\, q_S^{*F}/\Delta\, C_S^F$ is the slope of the chord for the less retained compound. If the feed concentration of the less retained compound is 2 $\mathrm{g/dm}^3$ then the term $\Delta\, q_S^{*F}/\Delta\, C_S^F$ is equal to 2.72 and the SMB flow rate in section 4 is 33.98 $\mathrm{cm}^3/\mathrm{min}$.

Considering the condition stated by the equilibrium theory in section 4 the following criterion must be fulfilled: $\gamma_4 < \gamma_{4,\max} = 1 - \varepsilon/\varepsilon(K_S + \varepsilon_p) = 4.965$ (where K_S is the initial slope of the isotherm for the less retained compound, $K_S = 2.86$) which corresponds to maximal SMB flow rate in section 4 equal to 36.19 $\mathrm{cm}^3/\mathrm{min}$.

The separation regions were constructed by repeating the following steps: feed flow rate, the interstitial velocity in section 2 was increased and hence the extract flow rate was decreased and raffinate increased in order to keep the mass balance of the system closed. To determine extract flow rate (Q_X) and raffinate flow rate (Q_R) with high accuracy to the boundaries of the separation region the interstitial velocity increment chosen was 0.01 cm/min.

With this approach the whole separation region for certain values of γ_1 and γ_4 was determined. The separation regions were constructed for purities of both products over 99%.

Separation Volumes for Different Particle Size

The separation regions for each value of γ_1 or γ_4 were constructed and shown in a three-dimensional projection $\gamma_1 \times \gamma_2 \times \gamma_3$ for constant values of γ_4 or with $\gamma_4 \times \gamma_2 \times \gamma_3$ space for constant values of γ_1, and also in a two-dimensional projection $\gamma_2 \times \gamma_3$ resulting from the evaluation of the 99% separation region, always considering the constant switching time period $t^* = 3.5$ min. The 2D projection, the common form of presentation of separation regions, was used in order to better observe the change of the size of triangles (separation region). It should be pointed out that in all figures the shaded area is representing the diagonal line from the 2D projection (no feed is introduced) and lines on the bottom and top of the graphs are the minimal value of γ_1 and maximum γ_4 given by equilibrium theory, respectively.

The separation volumes were constructed in order to evaluate the effect of the particle size used in the separation process on the choice of γ_1 and γ_4. The influence of γ_1 were studied at a constant value of $\gamma_4 = 4.600$ for all particle sizes used. The influence of γ_4 were studied at a constant value of $\gamma_1 = 5.757$ for particle sizes 20 μm and 40 μm. For the particle size 60 μm the value of $\gamma_1 = 5.922$ was chosen as the analysis with constant value of $\gamma_4 = 4.600$ has shown that for $\gamma_1 = 5.757$ does not exist any region for extract and raffinate the purities requirements above 99%. The other model parameters (particle size, average overall mass transfer, molecular diffusivity) are listed in Table 2.

The effects of choice of values of γ_1 at constant values of γ_4 and vice versa for the particle size 20 μm are shown in Fig. 7a and Fig. 8a, respectively. The obtained separation regions for the same cases in $\gamma_2 \times \gamma_3$ plane were plotted and they are shown in Fig. 7b and Figure 8b.

The separation volumes in 3D and 2D projection for the particle size 40 μm and 60 μm using the same strategy are reported in Figs. 9–12. Generally, it can be concluded that for all particle sizes, the separation regions are expanding by increasing γ_1 over the minimal value of $\gamma_{1,\min} = 5.715$ given by the equilibrium theory.

The expansion of the separation regions with increase of γ_1 above $\gamma_{1,\min}$ is not very visible in the case of particle size 20 μm (Figure 7a and 7b) since using this particle size the separation process is almost under the equilibrium control regime and the effect of the mass transfer resistance is negligible. The position of the vertex of the separation region is constant and not changing with further increment of γ_1 (see Fig. 7). The opposite situation can be noticed using particle size 60 μm. There is no separation region when for both products purities above 99% are required at $\gamma_1 = 5.757$ as for particle size 20 μm and 40 μm (see Figs. 11a and 11b). Also, it can be observed that the separation regions at $\gamma_1 < 5.922$ (Figs. 11a, and 11b) are occurring in transition region (51). The separation regions expand until a certain value of γ_1 ($\gamma_1 > 6.087$); further increasing of γ_1 will not affect the vertex position of separation region and only the desorbent consumption will increase.

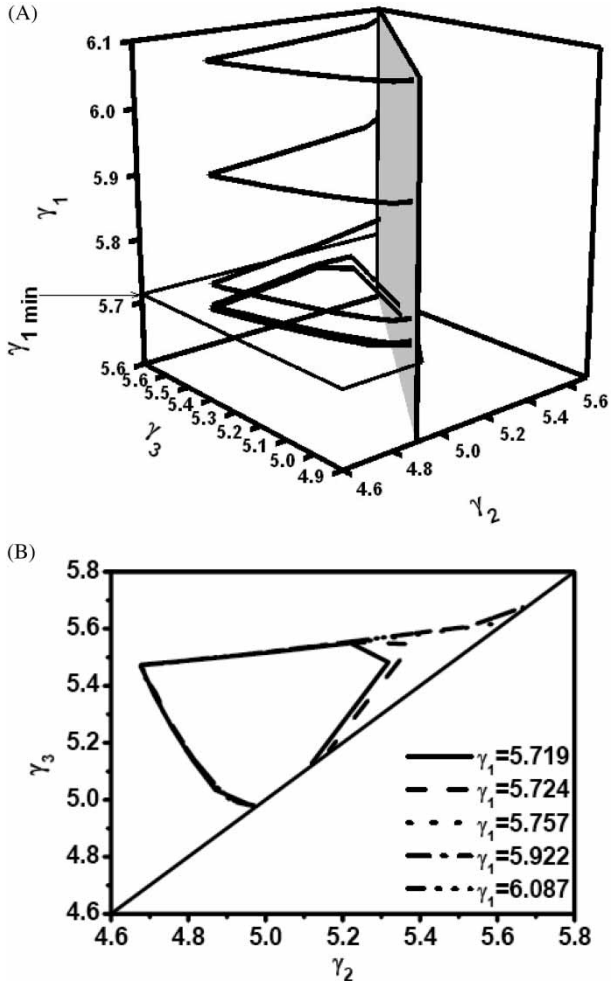

Figure 7. (a) 3D separation volume $\gamma_1 \times \gamma_2 \times \gamma_3$ where $\gamma_4 = 4.600$ for particle size 20 μm; (b) Separation region $\gamma_2 \times \gamma_3$ where $\gamma_4 = 4.600$ for varying γ_1 (particle size 20 μm).

If the value of γ_1 is fixed (γ_1= 5.757 for particle size 20 μm and 40 μm; $\gamma_1 = 5.922$ for particle size 60 μm) the separation region for all the particle sizes used are uniform until a particular value of γ_4. After this value of γ_4, the regions are decreasing and approaching the value $\gamma_{4,\max}$, given by the equilibrium theory, the separation regions are vanishing. Therefore it is preferred to work at a value of γ_4 where the separation region is unchanged but at the lowest eluent flow rate as possible, since the value of γ_4 is influencing the eluent consumption (39, 55, 56). In fact, the eluent consumption can be expressed as $SC = 1/C_F^S + C_F^R\,[1 + \gamma_1 - \gamma_4/\gamma_3 - \gamma_2]$.

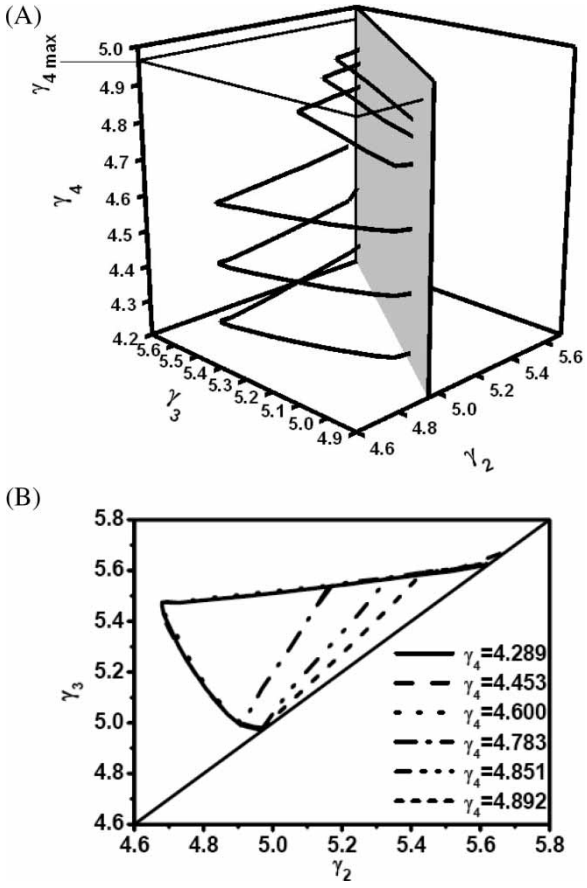

Figure 8. (a) 3D separation volume $\gamma_4 \times \gamma_2 \times \gamma_3$ where $\gamma_1 = 5.575$ for particle size 20 μm; (b) Separation region $\gamma_2 \times \gamma_3$ where $\gamma_1 = 5.757$ for varying γ_4 (particle size 20 μm).

The maximum productivity is achieved when the maximum feed flow rate is processed. This fact can be seen if we rewrite the productivity of the extract node or raffinate node, PR_X, PR_R (Eq. 26a, 26b) as a function of the recovery in a particular node and processed feed flow rate then productivity is given as follows: $PR_X = (\gamma_3 - \gamma_2)\varepsilon Q_s RE_X C_F^R/(1-\varepsilon)V_{ads}$; $PR_R = (\gamma_3 - \gamma_2)\varepsilon$ $_R = (\gamma_3 - \gamma_2)\varepsilon Q_s RE_R C_F^S/(1-\varepsilon)V_{ads}$. It is clear that the productivity of the particular node increase when there is maximum difference $\gamma_3 - \gamma_2$, the vertex.

As was pointed out before, with increase of γ_1 the difference $(\gamma_3 - \gamma_2)$ is also increasing, leading to higher SMB productivity values.

The productivities for all particle sizes used at the vertex of each separation region for constant value of γ_4 were calculated, and plotted as a function of γ_1 in Fig. 13.

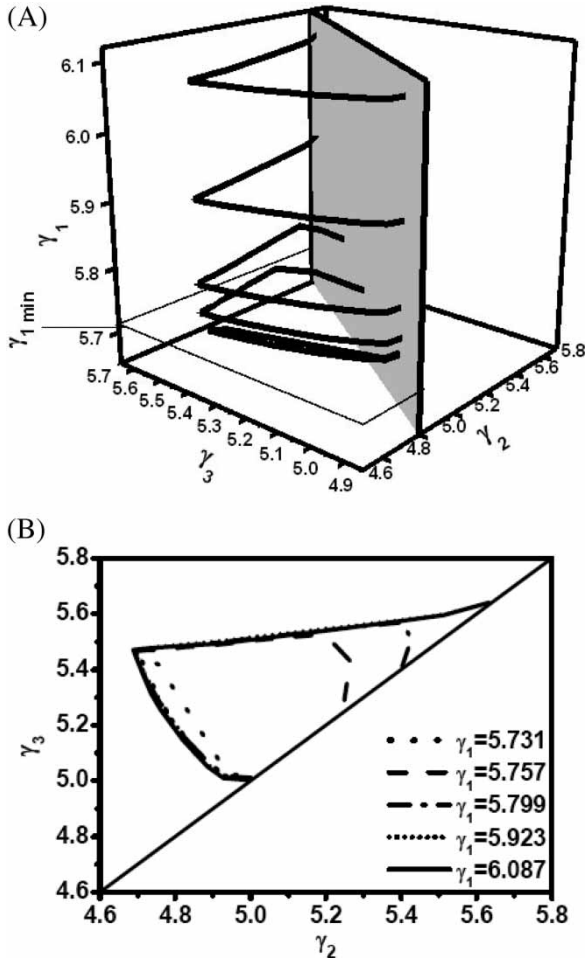

Figure 9. (a) 3D separation volume $\gamma_1 \times \gamma_2 \times \gamma_3$ where $\gamma_4 = 4.600$ for particle size 40 μm; (b) Separation region $\gamma_2 \times \gamma_3$ where $\gamma_4 = 4.600$ for varying γ_1 (particle size 40 μm).

It is clear that by using bigger particle sizes the influence of the mass transfer resistance is larger, therefore lower feed flow rates can be processed, and lower productivity will be obtained compared to smaller particles.

The eluent consumption was calculated for different values of γ_1 and constant value of $\gamma_4 = 4.600$ for each particle size used (Fig. 14). It can be seen that the dependence of the eluent consumption for the particle size 20 μm is nearly linear whereas for the particle sizes 40 μm and 60 μm is nonlinear and a minimum eluent consumption can be recognized. The lowest eluent consumption for particle size 20 μm, 40 μm, and 60 μm is

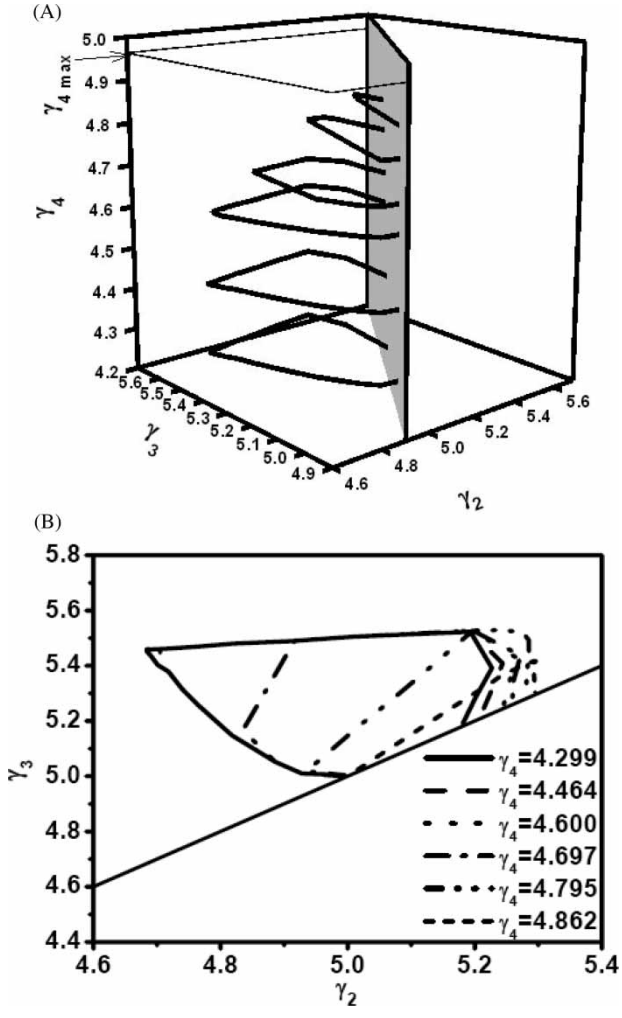

Figure 10. (a) 3D separation volume $\gamma_4 \times \gamma_2 \times \gamma_3$ where $\gamma_1 = 5.575$ for particle size 40 μm; (b) Separation region $\gamma_2 \times \gamma_3$ where $\gamma_1 = 5.757$ for varying γ_4 (particle size 40 μm).

obtained at values of γ_1 5.724, 5.757, and 5.881, respectively. It can be seen that values of γ_1 5.757, and 5.881 for particle size 40 μm. and 60 μm are higher than the lowest value of γ_1 (5.731 and 5.839 for particle sizes 40 μm and 60 μm, respectively) at which the first separation region for 99% product purities appears.

Figure 15 shows the productivities for both enantiomers of R,S-α-Tetralol and pressure drop as a function of the particle size. The pressure drop was calculated for the columns with dimensions 10 × 2.6 cm I.D.

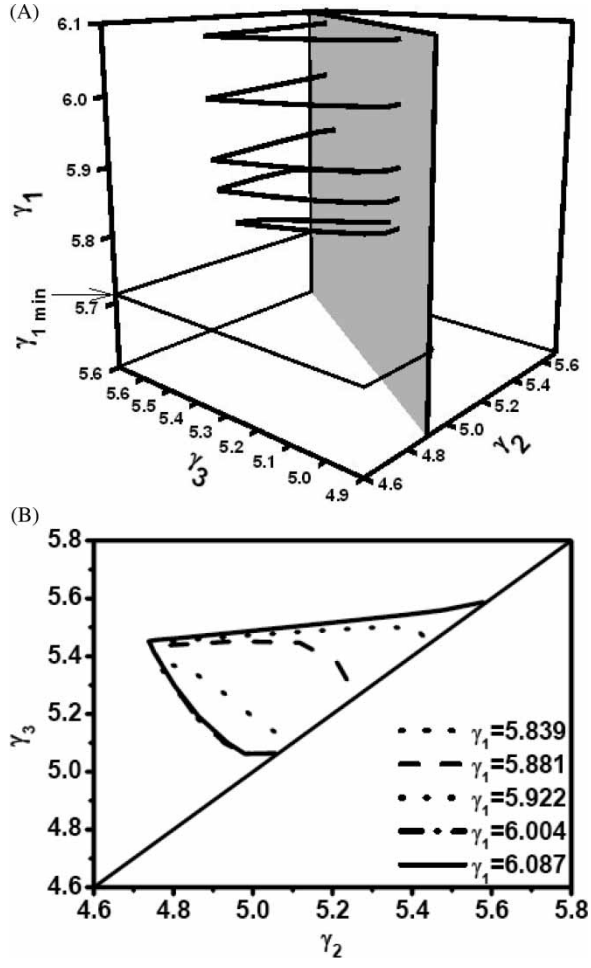

Figure 11. (a) 3D separation volume $\gamma_1 \times \gamma_2 \times \gamma_3$ where $\gamma_4 = 4.600$ for particle size 60 μm; (b) Separation region $\gamma_2 \times \gamma_3$ where $\gamma_4 = 4.600$ for varying γ_1(particle size 60 μm).

and at a flow rate 43.0 cm^3/min. Productivities were calculated at the vertex of the separation region for values of $\gamma_1 = 6.087$ and $\gamma_4 = 4.600$. The trends of productivity presented in Fig. 15 for both enantiomers and at the constant value of γ_1 ($\gamma_1 = 6.087$) show that the productivity is decreasing with increasing particle diameter as a result of higher mass transfer resistance. On the other hand, using bigger particle sizes for the separation purpose leads to lower pressure drop in the system, which allows processing of the higher feed flow rate, with a positive effect on productivity.

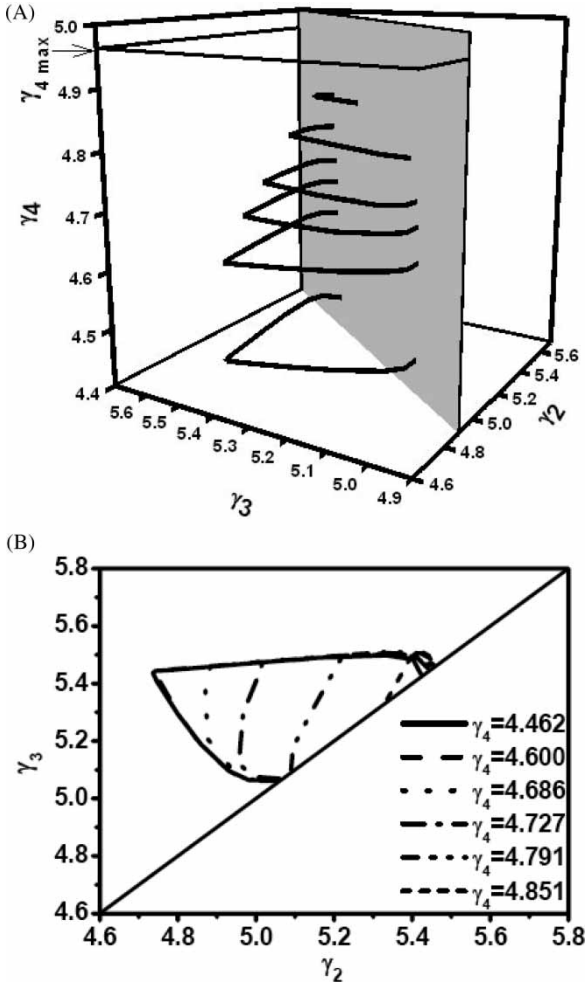

Figure 12. (a) 3D separation volume $\gamma_4 \times \gamma_2 \times \gamma_3$ where $\gamma_1 = 5.922$ for particle size 60 μm; (b) Separation region $\gamma_2 \times \gamma_3$ where $\gamma_1 = 5.922$ for varying γ_4 (particle size 60 μm).

EXPERIMENTAL SECTION

Operation of SMB System LICOSEP 12–26

In this section, only experimental results obtained with the chiral adsorbent CHIRALPAK AD (Chiral Technologies, France) with particle size 20 μm are presented for confidentiality reason.

All SMB experiments have been performed in a pilot unit LICOSEP 12–26 manufactured by Novasep (Vandoeuvre-dès-Nancy, France). The SMB

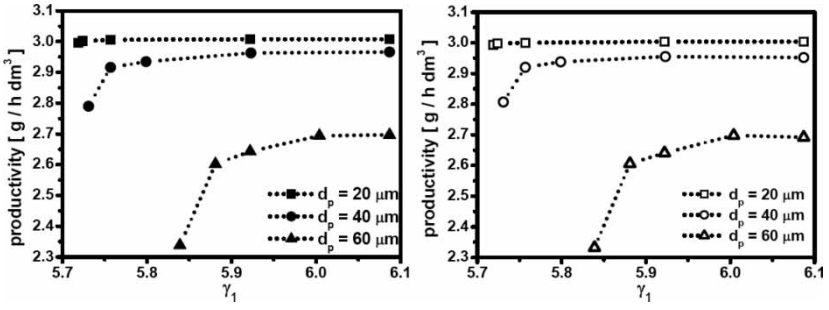

Figure 13. Productivities calculated at the vertex of each separation region for constant value of $\gamma_4 = 4.600$.

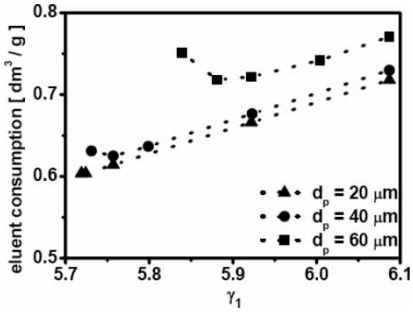

Figure 14. Eluent consumption calculated for constant value of $\gamma_4 = 4.600$.

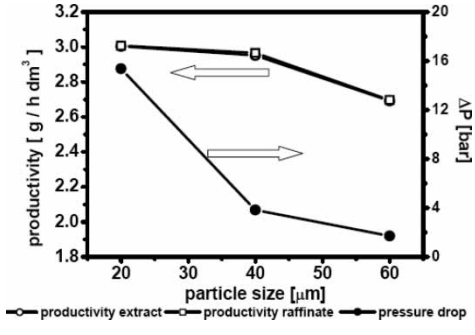

Figure 15. Comparison between the productivity and pressure drop vs. particle size.

system was operated with six and eight columns Superformance 100 × 26 (length × I.D., mm) (Götec Labortechnik, Germany) connected in series. The maximum allowable pressure for the columns is 60 bars. The packing procedure and characterization of all packed columns is described in the

next section. The operating temperature controlled by thermostat bath (Lauda, Germany) was 25ºC.

The inlets and outlets of the columns are connected by 24 two-way high-pressure pneumatic valves (TOP Industry, France), which by opening and closing at regular time intervals, switch the position of the inlet and the outlet streams. The unit is controlled by process control software (Novasep, France). The individual streams were pumped by four HPLC pumps model L-6000A and L-6200A (Merck-Hitachi, Germany). The maximum flow rate of the eluent and the extract pumps is $30\,cm^3/min$, raffinate, and feed pumps $10\,cm^3/min$. The recirculation of the eluent from section 4 to section 1 is carried out by a three-head membrane pump (Milton Roy, France), with a minimum flow rate 20 ml/min and a maximum flow rate 120 ml/min. The recycling pump flow rate is measured by turbine flowmeter (Hoffer Flow, USA) located at its outlet. In order to achieve a proper recycling flow rate the recycling pump and the flowmeter of the SMB system must be calibrated. The discharge pressure of the recycling pump is controlled by pressostat and the maximum pressure is set with respect to the maximum pressure of the columns. Pressure in the system is measured between the last column of the system and recycling pump. The system makes use of this pressure to control the extract flow rate. The internal liquid phase concentration profile in Licosep 12–26 is determined using 6-port valve, which is located before the first column. Tubings with $1/16''$ external and 1 mm internal diameter are used in order to minimize the dead volume of the system. Appropriate shifting of the injection and withdrawal points compensates the effect of dead volume of recycling pump, which delays the concentrations leaving the last column of the system and entering to the first column. In this manner they are not translated at a same time but shifted with delay t_d given by $t_d = 4V_d/\sum_{j=1}^{4} Q_j$.

Packing Procedure and Characterization of Individual Preparative Columns

The packing procedure, proposed by Nicoud (52) has been used. In order to get the desired column length the amount of packing material per column was 31.5 g; additional specifications regarding the packing procedure can be found elsewhere (41) The geometrical characteristic of all packed columns are listed in Table 3.

The preparative columns packed with CHIRALPAK AD elution were characterized by measuring of the pressure drop, total porosity of bed, enantioselectivity, and column efficiency.

The pressure drop over individual preparative columns packed with CHIRALPAK AD with particle size 20 μm has been measured. Due to hardware limitation of the HPLC system an external manometer has been connected. Each value of the pressure drop has been measured three times,

Table 3. Geometrical characteristic of the preparative columns (2.6 cm I.D.) filled with chiral adsorbent CHIRALPAK AD with particle size 20 μm

n	L [cm]	Relative error [%]	V [10^3 L]	ΔP [bar]	Relative error [%]	ε_T	Relative error [%]
I	10.04	−0.266	53.31	0.370	−7.872	0.624	1.109
II	9.96	0.533	52.88	0.454	−32.362	0.631	0.000
III	9.94	0.732	52.77	0.304	11.370	0.636	−0.792
IV	10.08	−0.666	53.52	0.330	3.790	0.637	−0.951
V	10.06	−0.466	53.41	0.383	−11.662	0.628	0.475
VI	10.00	0.133	53.09	0.363	−5.831	0.629	0.317
Average	10.01		53.16	0.367		0.631	
VII	10.00	0.224	53.09	0.367	0.811	0.625	0.833
VIII	10.10	−0.773	53.62	0.389	−5.135	0.632	−0.278
Average	10.02		53.21	0.370		0.630	

in order to decrease systematic error. Experimental pressure drop over individual preparative columns packed with chiral adsorbent CHIRALPAK AD are reported in Table 3. The relative error of experimental pressure drop from the theoretical pressure drop calculated at an average flow rate ($Q = 10 \pm 0.5\ \mathrm{cm}^3/\mathrm{min}$) was evaluated. Deviation of the theoretical and experiment pressure drop could be due to non-constant flow rate used, where the relative error of flow rate was 0.66%.

The total porosity of packed columns was measured with non-retained compound (1,3,5-Tri-tert-butylbenzene, TTBB). The experiments were carried out at a flow rate $10 \pm 0.5\ \mathrm{cm}^3/\mathrm{min}$ and at constant temperature (25°C). The calculated total porosities of all packed columns are reported in Table 3. Enantioselectivity and column efficiency was determinate by elution experiments using trans-Stilbene oxide enantiomers. The calculated retention factors $k = (t_R - t_0)/t_0$, where t_R and t_0 are retention times of retained enantiomers and non-retained compound (TTBB), respectively) for trans-Stilbene oxide for all packed columns are shown in Fig. 16. The values of total porosity of the individual columns and retention factors of trans-Stilbene oxide enantiomers are not significantly different from their average values.

The efficiency of individual preparative columns was characterized by the height equivalent to a theoretical plate (HETP). The HETP of enantiomers of trans-Stillbene oxide at flow rate $10 \pm 0.5\ \mathrm{cm}^3/\mathrm{min}$ was determinate. The calculated HETP for trans-Stilbene oxide are shown in Fig. 17. However, relative errors higher than 5% could be observed in HETP analysis, mainly due to second moments, which are generally known for their poor reproducibility arising from the errors caused by the signal noise in the end of the elution profile.

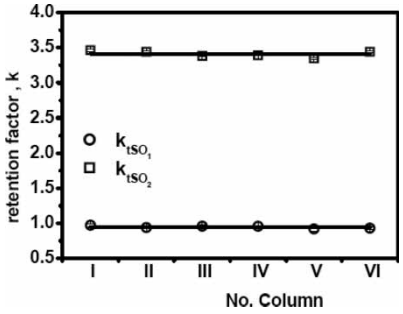

Figure 16. Retention factor for trans-Stillbene oxide enantiomers on the preparative column (2.6 cm I.D.) filled with chiral adsorbent CHIRALPAK AD. Mobile phase: n-Heptane/2-propanol (95/5) and temperature 25°C.

Separation of R,S-α-Tetralol Enantiomers using CHIRALPAK AD with Particle Size 20 μm

Determination of Operation Conditions

In this section, the results of the experiments performed in the SMB pilot plant Licosep 12–26 using CHIRALPAK AD with particle size 20 μm are presented.

The maximum operating pressure on preparative columns packed with CHIRALPAK AD (particle size 20 μm) was assumed to be 20 bar (57) and therefore the maximum liquid flow rate allowed in the SMB system was 41 cm^3/min for SMB system of 6 columns and 38 cm^3/min for SMB system of 8 columns. To satisfy the inequality of Eq. (28) the chosen switching time period must be greater than the retention time of more retained compound at a maximum flow rate in section 1. The retention time of more retained component in section 1 calculated by Eq. (32) and

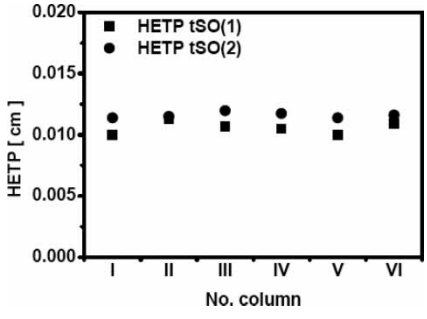

Figure 17. HETP of enantiomers of trans-Stillben oxide (tSO) on the preparative column (2.6 cm I.D.) packed with chiral adsorbent CHIRALPAK AD.

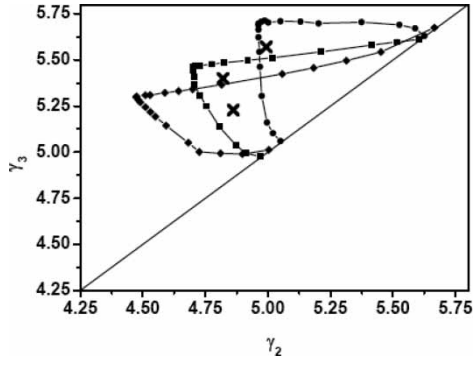

Figure 18. Separation regions at the total feed concentration 1.0 g/dm^3, 4.0 g/dm^3 (concentration is express per racemate). Cross points are the operating condition for individual SMB experiment.

considering configuration of 6 columns and 8 columns the maximum flow rates in section 1 are 3.47 min and 3.77 min, respectively and hence the switching time periods chosen were 3.5 min and 3.9 min, respectively.

For the selected switching time period ($t^* = 3.5$ min) the flow rate in the section 4 was approximated by Eq. (33) The SMB experiments with

Table 4. Experimental operating conditions in the linear part of equilibrium isotherm

	Sections (cm^3/min)			
	I	II	III	V
SMB condition	41.00	36.29	39.79	35.48
TMB condition	34.94	30.23	33.73	29.42
Eluent = 5.52 cm^3/min				
Extract = 4.71 cm^3/min				
Feed = 3.5 cm^3/min				
Raffinate = 4.31 cm^3/min				
Switching time = 3.5 min				
Solid flow rate = 9.08 cm^3/min				
Fluid and solid velocities ratio (equiv. TMB)				
$\gamma_1 = 5.771$				
$\gamma_2 = 4.993$				
$\gamma_3 = 5.571$				
$\gamma_4 = 4.859$				

Configuration: 1:2:2:1; No. Columns: 6 Columns: Length: 10.01 cm. Diameter: 2.6 cm. External porosity, $\varepsilon = 0.4$; Feed concentration:1.0 g/dm^3 (racemate); Particle size: 27 μm; $D_m = 2.8 \times 10^{-5}$ cm^2/s; $k_{ov} = 0.0042$ cm/s.

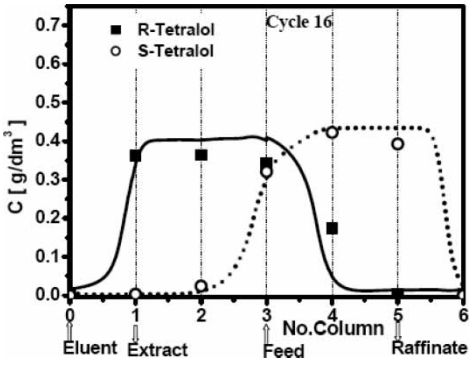

Figure 19. Experimental (points) and predicted (line) internal concentration profiles in cycle 16 at total feed concentration 1.0 g/dm^3.

configuration of 6 columns were carried out at total feed concentrations: 1.0 g/dm^3 and 4.0 g/dm^3 hence the term $\Delta q^{*F}_S/\Delta C^F_S$ Eq. (33) is equal to 2.89, 2.72, respectively. The SMB experiments with configuration of 8 columns were carried on at total feed concentrations 10.0 g/dm^3 thus the term $\Delta q^{*F}_S/\Delta C^F_S$ is equal to 2.45. Base on the above calculations the flow rates in section 4 are 35.50 cm^3/min ($C^{rac}_F = 1.0\ g/dm^3$) and 33.91 cm^3/min ($C^{rac}_F = 4.0\ g/dm^3$) for the SMB system with configuration of 6 columns and 28.45 cm^3/min ($C^{rac}_F = 10.0\ g/dm^3$) for the SMB system with configuration of 8 columns.

Using these constraints for sections 1 and 4 the separation regions were constructed. The obtained separation region for a given feed concentrations

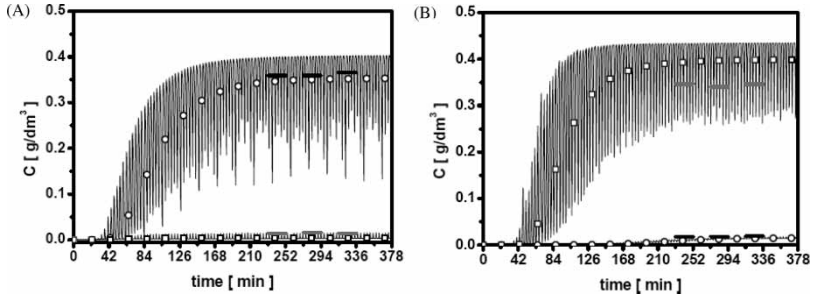

Figure 20. (a) Transient evolution of extract stream (full line) during 16 cycles with average concentration over the switching time interval (○–R-Tetralol, □–S-Tetralol) and experimental average concentration (— – R-Tetralol and — – S-Tetralol); (b) Transient evolution of raffinate stream (full line) during 16 cycles with average concentration over the switching time interval (○–R-Tetralol, □–S-Tetralol) and experimental average concentration (— – R-Tetralol and — – S-Tetralol).

Table 5. Comparison between the experimental (after 16th cycle) and predicted performance parameters in steady state

	Purity [%]		Recovery [%]	
Performance parameters	Extract	Raffinate	Extract	Raffinate
Simulated (Licosep model)	98.64	96.35	95.60	98.65
Experimental	96.17	94.49	92.98	90.86

used are shown in Fig. 18. The SMB experiments with configuration of 6 columns were carried out at the feed flow rate 3.50 cm^3/min and the SMB experiments with configuration of 8 columns were carried out at the feed flow rate 2.0 cm^3/min. The cross points in Fig. 18 are representing the individual operating conditions (see Tables 4, 6, 9)

Sample Withdrawing and Analysis

The SMB internal concentration profiles were determined by the collecting sample along the SMB columns at one quarter, half and three quarter of the switching time. The samples were collected at cyclic steady state at the end of each column using 6-port valve. Also, the extract and raffinate were

Table 6. Experimental operating conditions for feed concentration 4.0 g/dm^3

	Sections (cm^3/min)			
	I	II	III	V
SMB condition	41.00	35.27	38.77	34.09
TMB condition	34.94	29.21	32.71	28.03
Eluent = 6.91 cm^3/min				
Extract = 5.73 cm^3/min				
Feed = 3.5 cm^3/min				
Raffinate = 4.68 cm^3/min				
Switching time = 3.5 min				
Solid flow rate = 9.08 cm^3/min				
Fluid and solid velocities ratio (equiv. TMB)				
$\gamma_1 = 5.771$				
$\gamma_2 = 4.824$				
$\gamma_3 = 5.402$				
$\gamma_4 = 4.629$				

Configuration: 1:2:2:1 No. Columns: 6 Columns: Length: 10.01 cm Diameter: 2.6 cm. External porosity, $\varepsilon = 0.4$; Feed concentration:4.0 g/dm^3 (racemate); Particle size: 27 μm; $D_m = 2.8 \times 10^{-5}$ cm^2/s; $k_{ov} = 0.0042$ cm/s.

collected during whole cycle and the average extract and raffinate concentration was measured.

The samples were analyzed using the analytical column CHIRALCEL OBH (25 × 0.46 cm I.D.), supplied by Chiral Technologies, France. Eluent used was n-Heptane/2-propanol (95/5, v/v).

SMB Experiments

The SMB experiments were carried on a system free of separated species and equilibrated with pure eluent.

Feed Concentration 1.0 g/dm^3

Experimental operating condition for the feed concentration 1.0 g/dm^3 and model parameters are presented in Table 4. A comparison between the experimental points collected at half of the switching time and internal concentration profile predicted with Licosep model are reported in Fig. 19. Figures 20a, and b compare the transient evolution profiles of the Licosep model of the more retained species (R-α-Tetralol) and less retained species (S-α-Tetralol) in the extract stream and in the raffinate stream with average concentrations calculated over one cycle and average experimental concentrations of both species in the extract stream (R-α-Tetralol) and raffinate stream (S-α-Tetralol). The experimental samples were collected during the entire cycle.

The experimental SMB performance parameters calculated from the extract and raffinate average concentration in the 16th cycle, together with those predicted by Licosep model are presented in Table 5.

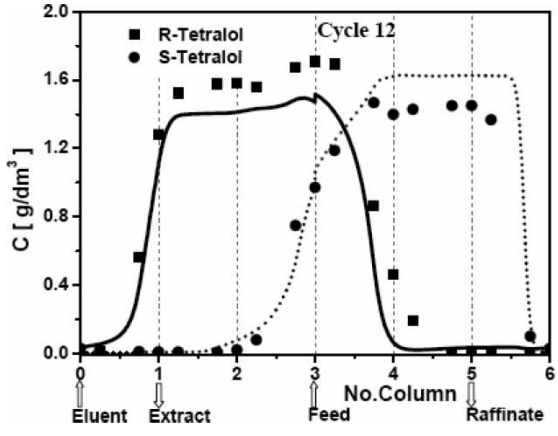

Figure 21. Experimental (points) and predicted (line) internal concentration profiles in cycle 12 at total feed concentration 4.0 g/dm^3.

Feed Concentration 4.0 g/dm³

Experimental operating condition for total feed concentration 4.0 g/dm³ (racemate) and model parameters are presented in Table 6 and shown in Fig. 18.

Experimental internal concentration profile is presented in Fig. 21; samples were collected at one quarter, half switching time and at three-quarters of the switching time. The transient evolution profile of the extract and raffinate composition predicted by the Licosep model and those obtained experimentally are presented in Fig. 22a, and b, respectively. Experimental determined SMB performance parameters and those predicted by Licosep models are summarized

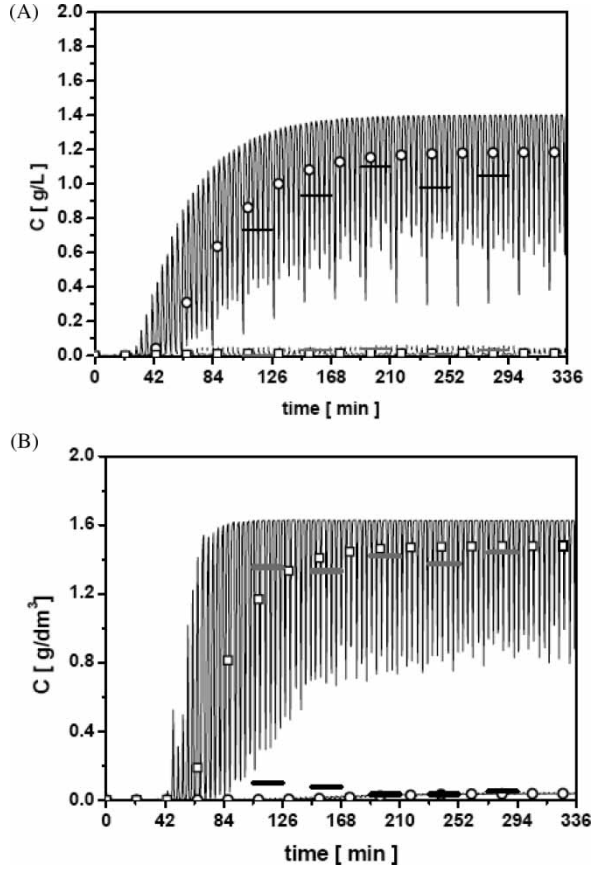

Figure 22. (a) Transient evolution of extract stream (full line) during 15 cycles with average concentration over the switching time interval (○–R-Tetralol, □–S-Tetralol) and experimental average concentration (— –R-Tetralol and — –S-Tetralol); (b) Transient evolution of raffinate stream (full line) during 15 cycles with average concentration over the switching time interval (○–R-Tetralol, □–S-Tetralol) and experimental average concentration (— –R-Tetralol and — –S-Tetralol).

Table 7. Comparison between the experimental (after 14th cycle) and predicted performance parameters incyclic steady state

	Purity [%]		Recovery [%]	
Performance parameters	Extract	Raffinate	Extract	Raffinate
Simulated (Licosep model)	98.81	97.55	97.50	98.83
Experimental	98.74	97.24	87.14	98.23

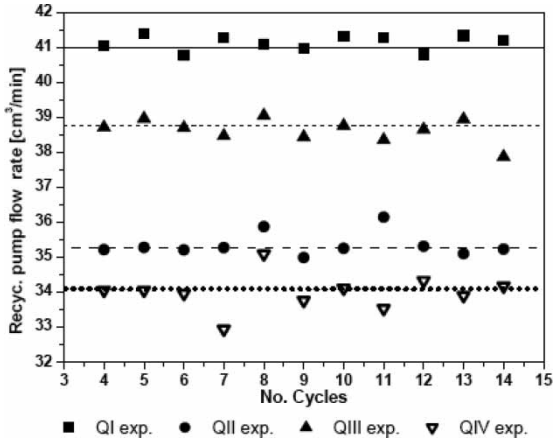

Figure 23. Recycling pump flow rates during the SMB experiment for chosen cycles. (Points are experimental flow rates and the lines are operating conditions Table 6).

in Table 7. There are noticeable differences between the model and the experimental results especially for the recovery in the extract stream (see Table 7). It seems that CSS was not reached in this experiment; Figure 22 shows that some perturbation occurred which led to a decrease in extract concentration in cycle12 and after CSS was not reached within 14 cycles.

Table 8. Dependence of performance parameters (purity and recovery) on recycling pump flow rate

		Purity [%]		Recovery [%]	
Error[%]	Q_{IV} [cm^3/min]	Extract	Raffinate	Extract	Raffinate
−3	33.067	93.33	91.94	91.79	93.43
−1	33.749	97.84	95.98	95.88	97.88
0	34.090	98.81	97.55	97.50	98.83
+1	34.431	99.12	98.70	98.61	99.14
+3	35.113	92.54	92.02	90.97	92.72

Table 9. Experimental operating conditions for feed concentration 10.0 g/dm^3

	Sections (cm^3/min)			
	I	II	III	IV
SMB conditions	38.00	31.95	33.95	29.1
TMB conditions	32.54	26.50	28.50	23.65
Eluent = 8.90 cm^3/min				
Extract = 6.05 cm^3/min				
Feed = 2.0 cm^3/min				
Raffinate = 4.85 cm^3/min				
Switching time = 3.92 min				
Solid flow rate = 8.18 cm^3/min				
Fluid and solid velocities ration (equiv. TMB)				
$\gamma_1 = 5.96$				
$\gamma_2 = 4.86$				
$\gamma_3 = 5.22$				
$\gamma_4 = 4.33$				

Configuration: 2:2:2:2 No. Columns: 8 Columns: Length:10.01 cm Diameter: 2.6 cm; External porosity, $\varepsilon = 0.4$; Feed concentration: 9.4 g/dm^3 (racemate); Particle size: 27 μm; $D_m = 2.8 \times 10^{-5}$ cm^2/s; $k_{ov} = 0.0042$ cm/s.

In fact there is some variation of the recycle flow rate which changes from cycle to cycle as shown in Fig. 23. Therefore, additional simulations were carried out to evaluate the effect of this variation on SMB performance. Table 8 shows how the variation on the recycle flow rate influences SMB

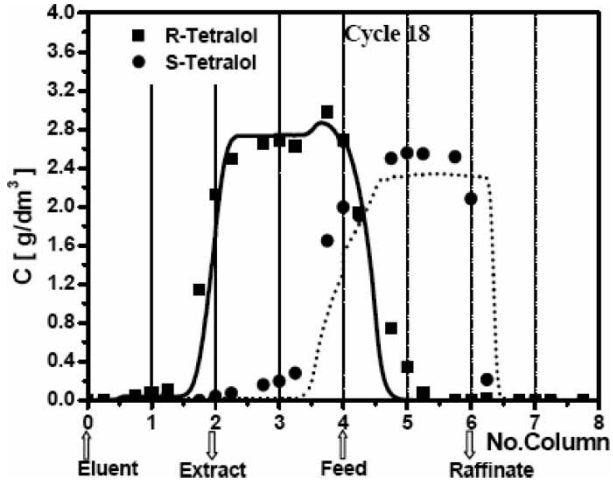

Figure 24. Experimental (points) and predicted (line) internal concentration profiles in cycle 18 at total feed concentration 9.4 g/dm^3 (8 columns configuration).

performance. The following errors in flow rate of the recycling pump were considered: $\pm$ 1.0% (Q_4^*= 33.75 cm^3/min; 34.43 cm^3/min) and $\pm$3.0% (Q_4^*= 33.07 cm^3/min; 35.11 cm^3/min). It can be noticed that by introducing error of 3% on the recycling pump flow rate the purities and recoveries on extract and raffinate side drastically decrease.

Feed Concentration 9.4 g/dm^3

Experimental operating conditions for total feed concentration 9.4 g/dm^3 (racemate) and model parameters are presented in Table 9 and shown in Fig. 18.

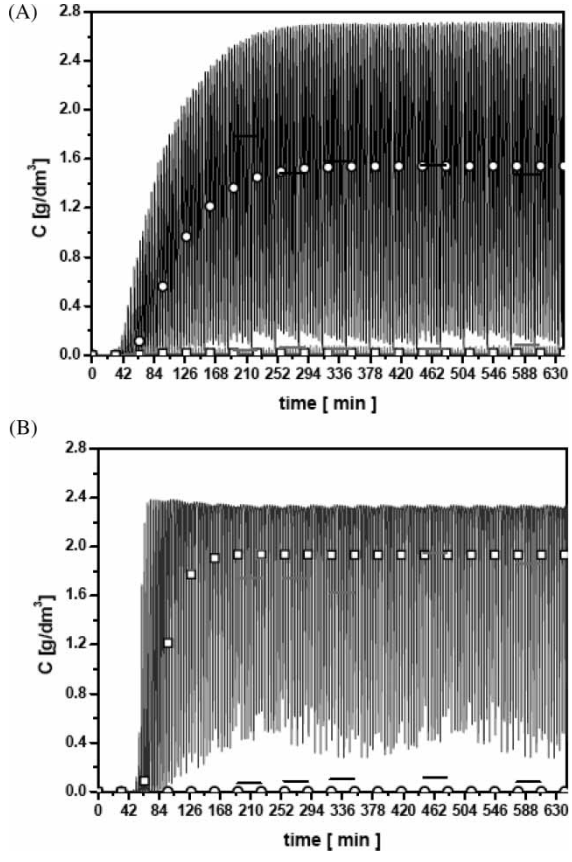

Figure 25. (a) Transient evolution of extract stream (full line) during 20 cycles with average concentration over the switching time interval (○–R-Tetralol, □–S-Tetralol) and experimental average concentration (— –R-Tetralol and — –S-Tetralol); (b) Transient evolution of raffinate stream (full line) during 20 cycles with average concentration over the switching time interval (○–R-Tetralol, □–S-Tetralol) and experimental average concentration (— –R-Tetralol and — –S-Tetralol).

Table 10. Comparison between the experimental (after 18th cycle) and predicted performance parameters in steady state

	Purity [%]		Recovery [%]	
Performance parameters	Extract	Raffinate	Extract	Raffinate
Simulated (Licosep model)	98.93	99.97	99.98	98.98
Experimental	94.32	95.91	95.19	94.67

Samples in experimental internal concentration profile presented in Fig. 24 in cycle 18 were collected at one quarter, half switching time and at three quarter of switching time. Transient evolution profiles of the extract and raffinate predicted by the Licosep model and those obtained experimentally are presented in Figs. 25a and b, respectively. Experimental determined performance parameters and those predicted by Licosep models are summarized in Table 10.

CONCLUSION

Influence of the particle size (mass transfer resistance) on the performance of SMB was investigated through simulation and experimentally. For this purpose, the SMB unit was modeled by the TMB and the SMB approach. The mathematical model considers non-linear the competitive adsorption isotherm, the axial dispersion, and the mass transfer resistance using linear driving force approximation.

The separation volume methodology was used to study the effect of the flow rates in section 1 and section 4 on the separation region when mass transfer resistance is significant. It was shown that by increasing the particle size (mass transfer resistance) the SMB productivity calculated in the vertex of the separation region decreases slightly; on the other hand the pressure drop in the system is significantly lower. The highest productivity was obtained for particle size 20 μm.

The typical linear dependence of eluent consumption on the γ_1 ratio found in equilibrium theory is not obtained if mass transfer resistance is present. Simulation results show that this dependence is becoming nonlinear as the mass transfer resistance is increasing and the minimum eluent consumption was obtained for certain γ_1 value.

The Licosep 12–26 SMB pilot plant was used to carry out the separation of the R,S-α-Tetralol on the CHIRALPAK AD with particle size 20 μm. The packed preparative columns were characterized in terms of pressure drop, total porosities, enantioselectivity, and separation efficiency. High reproducibility of the SMB columns packing allowed a good performance of SMB system.

The obtained purities and recoveries of both enantiomers of R,S-α-Tetralol were higher than 94% and in good agreement with those predicted with Licosep model. Experimental productivity using configuration of six columns at total feed concentration of 1 g/dm^3 was 0.52 g of R-α-Tetralol per dm^3 of adsorbent per hour and 0.47 g of S-α-Tetralol per dm^3 of adsorbent per hour, respectively. For the total feed concentration of 4.0 g/dm^3 the obtained productivity was 1.75 g R-α-Tetralol per dm^3 of adsorbent per hour and 2.03 g S-α-Tetralol per dm^3 of adsorbent per hour. Using configuration of eight columns at total feed concentration of 9.4 g/dm^3 the obtained productivity was 2.03 g of R-α-Tetralol per dm^3 of adsorbent per hour and 2.05 g of S-α-Tetralol per dm^3 of adsorbent per hour.

NOMENCLATURE

A	cross section area (m^2)
B_0	permeability (m^2)
b	equilibrium constant for the adsorption of enantiomers (m^3/kg)
C	bulk liquid phase concentration (kg/m^3)
C_0	initial (feed) concentration (kg/m^3)
$\bar{C}_p$	average pore liquid concentration (kg/m^3)
D_L	axial dispersion coefficient in packed bed (m^2/s)
d_c	diameter of the column (m)
d_p	diameter of particle (m)
D_m	molecular diffusion (m^2/s)
D_p	pore diffusion (m^2/s)
H	adsorption equilibrium constants of non-selective site (–)
K	adsorption equilibrium constants (–)
k_{ext}	external mass transfer coefficient (cm/s)
k_{int}	internal mass transfer coefficient (cm/s)
k_{ov}	overall mass transfer coefficient (cm/s)
L	column length (m)
M	molar mass of the solute (g/mol)
ΔP	column pressure drop (Pa)
$\bar{q}$	average adsorbed phase concentration (kg/m^3)
q^*	equilibrium adsorbed concentration (kg/m^3)
q_s	adsorbed phase saturation concentration of component (kg/m^3)
Q	liquid flow rate (m^3/s)
Q_s	solid flow rate (m^3/s)
R_p	particle radius (m)
Re	Reynolds number (–)
Sc	Schmidt number (–)
Sh	Sherwood number (–)
T	temperature (K)
t	time variable (s)

t^*	switching time (s)
t_R	retention time (s)
u_0	superficial velocity (m/s)
u_S	solid velocity (m/s)
v	interstitial velocity (m/s)
V	volume of the bed (m^3)
V_{ads}	volume of the adsorbent (m^3)
V_m	molar volume of the adsorbate at its normal boiling temperature (m^3/mol)
V_T	retention volume non-adsorbed tracer (m^3)
x	molar fraction (–)
z	axial variable (m)

Greek Letters

α	selectivity factor (–)
ε	external porosity (–)
ε_p	internal porosity (–)
ε_T	total porosity (–)
γ_j	ratio of fluid and solid velocity in section j
ϕ	association factor (–)
η	viscosity (Pa · s)
μ_1	first moment of the peak (s)
ρ	fluid density (kg/m^3)
σ^2	peak variance (s^2)
τ	tortuosity (–)

Subscripts and Superscripts

i	species in binary system
j	number of section ($j = 1,2,3,4$)
k	number of column ($k = 1,2, \ldots 6$)
pc	pipe connection in Licosep
*	operating conditions in SMB
E,F,R,X	eluent, feed, raffinate, extract TMB/SMB stream

ACKNOWLEDGMENTS

Michal Žabka (SFRH/BD/5418/2001) gratefully acknowledges the Ph.D grant from the "Fundação para a Ciência e Tecnologia." This work was financially supported by the project POCTI/EQU/59296/2004 ("Fundação para a Ciência e Tecnologia").

Chiral Technologies Europe is gratefully acknowledged by supplying the chiral adsorbent.

REFERENCES

1. Ruthven, D.M. and Ching, C.B. (1989) Countercurrent and simulated countercurrent adsorption separation processes. *Chem. Eng. Sci.*, 44 (5): 1011.
2. Broughton, D.B. and Gerhold, C.G. (1961) Continuous Sorption Process Employing Fixed Bed of Sorbent and Moving Inlets and Outlets. U.S. Patent No. 2,985,589.
3. Francotte, E.R. (2001) Enantioselective chromatography as a powerful alternative for the preparation of drug enantiomers. *J. Chromatogr. A.*, 906 (1–2): 379.
4. Francotte, E. (1994) Contribution of preparative chromatographic resolution to the investigation of chiral phenomena. *J. Chromatogr. A.*, 666 (1–2): 565.
5. Okamoto, Y., Aburatani, R., Fukumoto, T., and Hatada, K. (1987) Chromatographic resolution .17. Useful chiral stationary phases for Hplc - amylose tris(3,5-dimethylphenylcarbamate) and tris(3,5-dichlorophenylcarbamate) supported on silica-gel. *Chem. Lett.*, 9: 1857.
6. Okamoto, Y. and Yashima, E. (1998) Polysaccharide derivatives for chromatographic separation of enantiomers. *Angew. Chem.-Int. Edit.*, 37 (8): 1021.
7. Okamoto, Y. and Hatada, K. (1998) Alkyl-Phenylcarbamate Derivative of Polysacharide, Daicel Chemical Industries Ltd, EP0281951.
8. Okamoto, Y. and Hatada, K. (1989) Alkyl-Phenylcarbamate derivative of polysacharide, Daicel Chemical Industries Ltd. US, 4,861,872.
9. Yamashita, A. and Fumihiko, S. (1992) Process for Separating Optical Isomers, Daicel Chemical Industries Ltd. US 5,126,055.
10. Negawa, M. and Shoji, F. (1992) Optical resolution by simulated moving-bed adsorption technology. *Journal of Chromatography*, 590 (1): 113.
11. Nicoud, R.M., Bailey, M., Kinkel, J.N., Devant, R.M., Hampe, T.R., and Küsters, E. (1993) Simulated moving bed (SMB): Applications for enantiomer separations on chiral stationary phases, R.M. Nicoud, *Simulated Moving Bed: Basics and Applications*, INPL: Nancy, France, 65.
12. Charton, F. and Nicoud, R.M. (1995) Complete design of a simulated moving-bed. *J. Chromatogr. A.*, 702 (1–2): 97.
13. Negawa, M. and Shoji, F. (1995) Process for Recovering Optical Isomers and Solvent, Process for Using Solvent by Circulation and Process for Reusing Optical Isomers in Optical Resolution. US Patent 5,434,299.
14. Negawa, M. and Shoji, F. (1995) Simulated moving bed separation system, US Patent 5,46,825.
15. Schulte, M. and Strube, J. (2001) Preparative enantioseparation by simulated moving bed chromatography. *J. Chromatogr. A.*, 906 (1–2): 399.
16. Pais, L.S. (1999) *Chiral Separation by Simulated Moving Bed Chromatography*; University of Porto: Porto.
17. Pais, L.S., Loureiro, J.M., and Rodrigues, A.E. (2000) Chiral separation by SMB chromatography. *Sep. Purif. Tech.*, 20 (1): 67.
18. Zhang, Z., Hidajat, K., Ray, A.K., and Morbidelli, M. (2002) Multiobjective optimization of SMB and varicol process for chiral separation. *AIChE J.*, 48 (12): 2800.
19. Schulte, M., Kinkel, J.N., Nicoud, R.M., and Charton, F. (1996) Simulated moving-bed chromatograph - An efficient technique to producing opticaly active compounds on an industrial scale. *Chem. Ing. Tech.*, 68 (6): 670.
20. Miller, L., Orihuela, C., Fronek, R., Honda, D., and Dapremont, O. (1999) Chromatographic resolution of the enantiomers of a pharmaceutical intermediate from the milligram to the kilogram scale. *J. Chromatogr. A.*, 849 (2): 309.

21. Jupke, A., Epping, A., and Schmidt-Traub, H. (2002) Optimal design of batch and simulation moving bed chromatographic separation processes. *J. Chromatogr. A.*, 944 (1–2): 93.
22. Miller, L., Grill, C., Yan, T., Dapremont, O., Huthmann, E., and Juza, M. (2003) Batch and simulated moving bed chromatographic resolution of a pharmaceutical racemate. *J. Chromatogr. A.*, 1006 (1–2): 267.
23. Wongso, F., Hidajat, K., and Ray, A.K. (2004) Optimal operating mode for enantioseparation of SB-553261 racemate based on simulated moving bed technology. *Biotechnology and Bioengineering.*, 87 (6): 704.
24. Wongso, F., Hidajat, K., and Ray, A.K. (2005) Improved performance for continuous separation of 1,1′-bi-2-naphthol recemate based on simulated moving bed technology. *Sep. Purif. Tech.*, 46 (3): 168.
25. Biressi, G., Ludemann-Hombourger, O., Mazzotti, M., Nicoud, R.M., and Morbidelli, M. (2000) Design and optimisation of a simulated moving bed unit: role of deviations from equilibrium theory. *J. Chromatogr. A.*, 876 (1–2): 3.
26. Lee, K.B., Chin, C.Y., Xie, Y., Cox, G.B., and Wang, N.H.L. (2005) Standing-wave design of a simulated moving bed under a pressure limit for enantioseparation of phenylpropanolamine. *Industrial & Engineering Chemistry Research.*, 44 (9): 3249.
27. Zhang, Z., Mazzotti, M., and Morbidelli, M. (2003) Multiobjective optimization of simulated moving bed and Varicol processes using a genetic algorithm. *J. Chromatogr. A.*, 989 (1): 95.
28. Ludemann-Hombourger, O., Bailly, M., and Nicoud, R.M. (2000) Design of a simulated moving bed: Optimal particle size of the stationary phase. *Sep. Sci. Technol.*, 35 (9): 1285.
29. Pais, L.S., Loureiro, J.M., and Rodrigues, A.E. (1998) Modeling strategies for enantiomers separation by SMB chromatography. *AIChE J.*, 44 (3): 561.
30. Glueckauf, E. (1955) Theory of chromatography .10. Formulae for diffusion into spheres and their application to chromatography. *Transactions of the Faraday Society.*, 51 (11): 1540.
31. Wilke, C.R. and Chang, P. (1955) Correlation of diffusion coefficients in dilute solutions. *AIChE J.*, 1 (2): 264.
32. Perkins, L.R. and Geankoplis, C.J. (1969) Molecular diffusion in a ternary liquid system with diffusing component dilute. *Chem. Eng. Sci.*, 24 (7): 1035.
33. Teja, A.S. and Rice, P. (1981) Generalized corresponding states method for the viscosities of liquid-mixtures. *Ind. Eng. Chem. Fundam.*, 20 (1): 77.
34. Reid, R.C., Prausnitz, J.M., and Poling, B.E. (1987) *Properties of Gas and Liquids*; McGraw Hill: New York.
35. Gomes, P.S. (2007) Effect of dead volume on performance of the SMB unit Licosep 12–26 (personal communication) .
36. Migliorini, C., Mazzotti, M., and Morbidelli, M. (1999) Simulated moving-bed units with extra-column dead volume. *AIChE J.*, 45 (7): 1411.
37. Levenspiel, O. (1999) *Chemical Reaction Engineering*, 3rd edn.; John Wiley & Sons; U.S.A.
38. gPROMS (2003) *gPROMS v2.2 User Guide*. Process System Enterprise Ltd.
39. Minceva, M. and Rodrigues, A.E. (2002) Modeling and simulation of a simulated moving bed for the separation of p-xylene. *Ind. Eng. Chem. Res.*, 41 (14): 3454.
40. Zabka, M. (2006) Chiral separation by simulated moving bed and novel adsorbent structures. Ph.D. thesis, University of Porto: Porto.

41. Zabka, M. and Rodrigues, A.E. (2007) Measurement of pore diffusivity of R,S-[alpha]-Tetralol enantiomers in chiral adsorbent CHIRALPAK AD by zero length column method. *Sep. Purif. Tech.*, 57 (1): 74.
42. Ma, Z. and Wang, N.-H.L. (1997) Standing wave analysis of SMB chromatography: linear systems. *AIChE Journal.*, 43 (10): 2488.
43. Chiang, A. (1998) Complete separation conditions for a local equilibrium TCC adsorption unit. *AIChE J.*, 44 (2): 332.
44. Chiang, A.S.T. (1998) Continuous chromatographic process based on SMB technology. *AIChE Journal.*, 44 (8): 1930.
45. Storti, G., Masi, M., and Morbidelli, M. (1989) *Optimal Design of Simulated Moving Bed Adsorption Separation Units through Detailed Modeling and Equilibrium Theory*; Rodrigues, A.E., LeVan, M.D. and Tondeur, D. (eds.); Adsorption Science and Technology: Kluwer London, pp. 357.
46. Storti, G., Mazzotti, M., Morbidelli, M., and Carrá, S. (1993) Robust design of binary countercurrent adsorption separation processes. *AIChE J.*, 39 (3): 471.
47. Mazzotti, M., Storti, G., and Morbidelli, M. (1996) Robust Design of countercurrent adsorption separation: 3. nonstoichiometric systems. *AIChE J.*, 42 (10): 2784.
48. Mazzotti, M., Storti, G., and Morbidelli, M. (1997) Optimal operation of simulated moving bed units for nonlinear chromatographic separations. *J. Chromatography A.*, 769: 3.
49. Mazzotti, M., Storti, G., and Morbidelli, M. (1994) Robust design of countercurrent adsorption separation processes: 2. Multicomponent systems. *AIChE Journal.*, 40 (11): 1825.
50. Ma, Z. and Wang, N.H.L. (1997) Standing wave analysis of SMB chromatography: Linear systems. *AIChE J.*, 43 (10): 2488.
51. Azevedo, D.C.S. and Rodrigues, A.E. (1999) Design of a simulated moving bed in the presence of mass-transfer resistances. *AIChE J.*, 45 (5): 956.
52. Nicoud, R.M. (1993) A packing procedure suitable for high flow rate and high stability columns using cellulose triacetate. *LC-GC Int.*, 6: 636.
53. Rodrigues, A.E., Lu, Z.P., Loureiro, J.M., and Pais, L.S. (1995) Separation of enantiomers of 1a,2,7,7a-tetrahydro-3-methoxynaphtha-(2,3b)-oxirane by liquid-chromatography - laboratory-scale elution chromatography and modeling of simulated moving-bed. *J. Chromatogr. A.*, 702 (1–2): 223.
54. Mazzotti, M., Storti, G., and Morbidelli, M. (1997) Optimal operation of simulated moving bed units for nonlinear chromatographic separations. *J. Chromatogr. A.*, 769 (1): 3.
55. Minceva, M. and Rodrigues, A.E. (2005) Two-level optimization of an existing SMB for p-xylene separation. *Comput. Chem. Eng.*, 29 (10): 2215.
56. Rodrigues, A.E. and Pais, L.S. (2004) Design of SMB chiral separations using the concept of separation volume. *Sep. Sci. Technol.*, 39 (2): 245.
57. Chiral Technologies Europe. (2003) Guidelines for Daicel chiral stationary phases in preparative chromatography.